THE VESUVIUS DEM: A TEST CASE FOR THE TOPSAR SYSTEM

G. Alberti, S. Esposito, and S. Vetrella
CO.RI.S.T.A.
P.le Tecchio, 80 - 80125 Napoli (Italy)

ABSTRACT

This paper presents the analysis of the C-band cross-track interferometric data (XTI) acquired during the MAC-Europe 1991 campaign over the Vesuvius test-site in Southern Italy.
The main technical aspects of the end-to-end processing system, from raw data compression to digital elevation model (DEM) generation and validation, have been dealt with.
The interferometric data set has been compressed by using a range-Doppler SAR processor and the two images have been registered by using a one dimensional cross-correlation technique.
A new path independent and automatic method has been tested to unwrap the phase of the resulting interferogram.
The DEM, output of the end-to-end processing system, has been compared to the Istituto Geografico Militare Italiano (IGMI) DEM, slant-range projected by using a simulation program.
The resulting height rms error has been critically analysed by means of a theoretical error budget.

INTRODUCTION

The possibility of reconstructing terrain height by means of SAR interferometry has been successfully demonstrated in recent years (Refs. 1, 2). Several elevation maps have been derived either from data provided by satellite multiple-passes or by means of two antennas mounted on the same aeroplane (Refs. 3, 4, 5). Single-pass SAR interferometry overcomes surface temporal decorrelation and offers the potentiality of improving the accuracy over larger areas in comparison to multiple passes.
The latter has been proved by the TOPSAR, which is the interferometric system recently added (Ref. 5) to the NASA DC-8 airborne SAR (AVIOSAR). The Italian Consortium of Research on Advanced Remote Sensing Systems (CO.RI.S.T.A.) collaborated with JPL in the design of the new system and provided, under a contract with the Italian Space Agency (ASI), the pair of interferometric antennas.
During 1991 a large amount of interferometric data have been acquired by this system in U.S and Europe and various topographic maps have been derived.
The evaluation of the TOPSAR height accuracy has been performed by processing the Matera test-site (Italy) data and by comparing points of interferometric DEM with the height of homologous points corresponding to on-ground calibrators (Ref. 6).
More extensive validations have been performed by using, as a reference, available photogrammetric DEMs of Fort Irwin and Walnut Gulch American test-sites. In refs. 5 and 7 the interferometric DEM has been registered with respect to the photogrammetric one by a non-linear transformation which requires several tie-points. This approach, in addition to the well-known problem of identifying suitable control points, is not able to take into account and correct all the geometric deformations which are peculiar of SAR observation geometry.
Following a short description of the TOPSAR campaign and the interferometric processing approach, a new procedure to register the interferometric DEM to the photogrammetric one will be presented and the height accuracy will be critically analysed with respect to the theoretical error budget.

TOPSAR DATA PROCESSING

In the framework of the multisensor airborne campaign MAC Europe 1991, interferometric data have been acquired by the TOPSAR over the Italian test-sites of Montespertoli, Matera and Vesuvius.
The Vesuvius test-site has been covered on June 28 with two Northwest ascending flights..
Table 1 gives the main nominal system characteristics, during the data acquisition.

Frequency	5.2875 GHz
Wavelength, λ	5.67 cm
Baseline $\|B\|$	2.583 m
B_x	0
B_y	1.1821 m
B_z	2.2969 m
Aircraft speed	~ 211 m/s
Altitude, *H*	~ 7650 m
Slant range resolution	3.75 m
Azimuth resolution	0.8 m (1 look)
Chirp bandwidth	40 MHz
Pulse length	5.0 μs
Sampling frequency	90 MHz
PRF	567 Hz

Table 1. TOPSAR system main nominal characteristics

Figure 1 shows the ground flight path over the test area, which extends over more than 35 Km^2 and includes various land covers such as lava, vegetation and man-made features.
The morphology of the area is very complex, ranging from about 50 meters in the western part up to 1200 meters corresponding to the Vesuvius top.
The end-to-end processing system mainly consists of four successive steps: raw data compression, interferogram formation, phase unwrapping and DEM generation.
Each range line, consisting of 2800 real samples, has been calibrated by means of the calibration tone injected in the transmitted signal, and then compressed by using a range reference function which emulates the digital chirp generator

(DCG). A 1:2 presumming has been used to compress the 16384 range lines covering the test-site.
Figure 2 shows the high values of the Doppler centroid due to the aeroplane attitude, its variation from near to far range and the least-square approximation.
The analysis of the flight ancillary data has shown a satisfactory stability which did not require the application of the motion compensation algorithm.

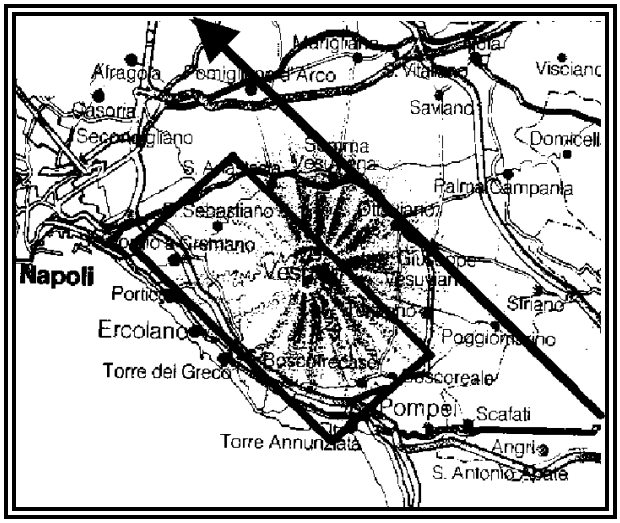

Figure 1. Map of the Vesuvius test-site

Therefore, a range-Doppler algorithm, which takes into account the range migration effect and the variation of the transmitting antenna Doppler centroid and rate, has been applied to both channels, to get the two images along-track registered.

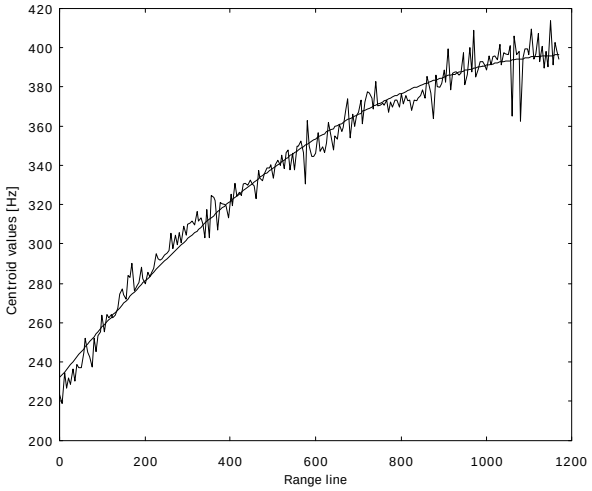

Figure 2. Estimated Doppler centroid variation along the swath and its least-square approximation.

Consequently, only a one dimensional sub-pixel registration along the range direction has been applied to form the interferogram, by using a cross-correlation technique.
The coherence of the resulting interferogram (figure 5) is very high (figure 6), except few small areas corresponding to thermal noise, shadow (Vesuvius vent), vegetation (Monte Somma slopes) and rapid variation of terrain height.

The most critical step of the end-to-end interferometric processing is phase unwrapping as shown by several authors (Refs. 8, 9 and 10).
A new consistent and completely automatic algorithm has been implemented and successfully tested on the Vesuvius test-site.
After the identification of phase local errors, the proposed algorithm is able to locate connex areas of low coherence, grouping the negative and positive residues, by enlarging an adaptive research window around each residue.
The final result is shown in figure 7, where the Vesuvius vent and a layover area have been well bounded and correspond to the two black areas on the image.
After unwrapping, the DEM has been derived by using the position and height of a ground control point to solve the 2π ambiguity, the altitude and attitude of the aeroplane, the baseline components and slant range (figures 8 and 9).

THEORETICAL ERROR BUDGET

The interferometric height (h) is a function of aircraft altitude (H), slant range (r), baseline components (B_y and B_Z), attitude angles (roll α and pitch β), interferometric phase (Φ), wavelength (λ) and look angle (θ), according to the following relations:

$$\begin{cases} h = H - r\cos\beta\sin(\vartheta + \alpha) \\ \Phi \approx \dfrac{2\pi}{\lambda}\left(B_z\cos\vartheta - B_y\sin\vartheta\right) \end{cases}$$

The height accuracy is then given by:

$$\sigma_h^2 = \left(\frac{\partial h}{\partial H}\right)^2\sigma_H^2 + \left(\frac{\partial h}{\partial r}\right)^2\sigma_r^2 + \left(\frac{\partial h}{\partial B_y}\right)^2\sigma_{B_y}^2 + \left(\frac{\partial h}{\partial B_z}\right)^2\sigma_{B_z}^2 + \left(\frac{\partial h}{\partial \Phi}\right)^2\sigma_\Phi^2 + \left(\frac{\partial h}{\partial \alpha}\right)^2\sigma_\alpha^2 + \left(\frac{\partial h}{\partial \beta}\right)^2\sigma_\beta^2$$

where:

$$\frac{\partial h}{\partial H} = 1$$

$$\frac{\partial h}{\partial r} = -\cos\beta\cos(\vartheta+\alpha)$$

$$\frac{\partial h}{\partial B_y} = \frac{rp\sin\vartheta}{q}$$

$$\frac{\partial h}{\partial B_z} = \frac{-rp\cos\vartheta}{q}$$

$$\frac{\partial h}{\partial \Phi} = \frac{-rp}{kq}$$

$$\frac{\partial h}{\partial \alpha} = r\cos\beta\sin(\vartheta+\alpha)$$

$$\frac{\partial h}{\partial \beta} = r\sin\beta\cos(\vartheta+\alpha)$$

$$p = \cos\beta\sin(\vartheta+\alpha)$$

$$q = B_z\sin\vartheta + B_y\cos\vartheta$$

$$k = \frac{2\pi}{\lambda}$$

The mean value, accuracy and multiplication factors of the above parameters are normally computed on the basis of the middle swath look angle. In case of α, β and H, the mean values and standard deviations are derived from the analysis of the flight ancillary data. The Cramer-Rao bound is applied to determine the phase accuracy as a function of the number of looks (N_L) and the coherence coefficient (γ) (Ref. 11):

$$\sigma_\Phi^2 = \frac{1-\gamma^2}{2N_L\gamma^2} \qquad (1)$$

DEM SLANT-RANGE PROJECTION

A digital elevation model enables a direct validation of the interferometric DEM, which is easier than the approach of using scattered ground control points and more accurate, provided that a precise registration and contour-level to raster format conversion are performed. The IGMI produces digital topographic data by digitising control points and contour levels of existing 1:25000 maps. A computer program allows to obtain the terrain elevation and slope in a digital raster format, using the digitised points as input (Ref. 12). This is performed by using a finite element method, by dividing the input elevation image in cells, where the altitude profile is given by a 4-th order polynomial depending on 12 coefficients.

The comparison between the interferometric and the reference DEMs can be performed either in geographic (Universal Transverse Mercator, UTM) or SAR (slant range and azimuth) coordinates.

The existing polynomial techniques are not able to adapt themselves to the complex geometric distortion due to SAR observation geometry, resolution and morphology of the area.

Consequently, the authors have implemented a computer program which, by simulating the aeroplane flight path and attitude and the SAR observation geometry, overcomes the above mentioned problems and allows an accurate registration and an extensive comparison between the two DEMs.

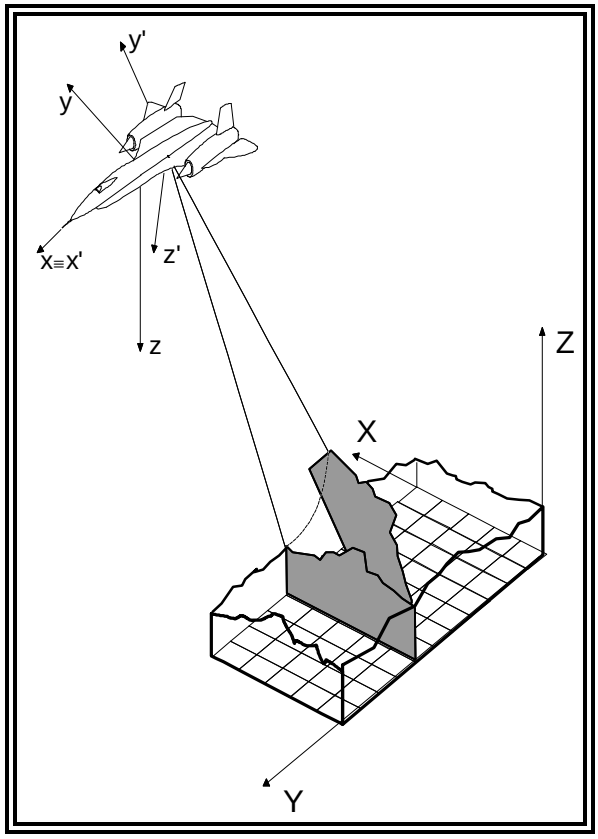

Figure 3. DEM projection geometry.

The flight path and attitude are given as a user defined function of time, derived by flight ancillary data processing.

For each azimuth position, the intersection of the antenna elevation plane with the geographic DEM is evaluated, to identify the geographic coordinates of each slant range sample. To this end, the time-variant transformation matrices between the dynamic reference frame (centred in the aircraft centre of mass, xyz) and the antenna reference frame (centred in the antenna phase centre, x'y'z') are computed (figure 3).

VALIDATION RESULTS

The interferometric DEM validation is performed in the following with respect to the framed area shown on the compressed SAR image of figure 4, where both the theoretical error budget and the comparison with the georeferenced photogrammetric DEM have been evaluated. This area represents a suitable validation test due to its extension (more than 13 km^2) and height variation (from 50 to 1016 m).

On the basis of the IGMI 1:25000 digitised map and the procedure previously described, a raster DEM has been derived as input to the simulation program in order to provide the slant-range DEM to compare with the interferometric one.

A 2.5 m rms error has been computed by comparing IGMI digitised contour levels and control points with the homologous points of the raster DEM. A total rms error of

3.9 m has been then obtained, by independently adding the standard accuracy of a 1:25000 map.
The simulation of the aeroplane dynamics, conducted on the basis of the processed ancillary data, has been used to identify a preliminary correspondence between a slant range line and the homologous line of the raster DEM. Residual registration errors due to the level of accuracy of ancillary data, have been corrected by means of a bidimensional correlation procedure. The final slant range projected IGMI DEM is shown in figure 10 and the registration accuracy of two homologous azimuth and range lines can be qualitatively evaluated in figures 11 and 12.
The comparison has been performed on more than one hundred thousand points, which represent the total test-area without the points eliminated by the phase unwrapping procedure. Figure 13 shows a mean height error of -39 m with a variance of 26 m.
To gain further insight into the interpretation of the validation test, a theoretical error of 18 m has been computed following the approach previously described.
Table 2 lists the accuracy and multiplication factor values for each parameter, computed on the basis of the first column mean values.

	$\bar{\bullet}$	$\left(\frac{\partial h}{\partial \bullet}\right)^2$	$\sigma_\bullet^2$
H	7650 m	1	2.6
r	10819 m	0.5	$O(10^{-1})$
B_y	1.1821 m	10^7	$O(10^{-7})$
B_z	2.2969 m	10^7	$O(10^{-7})$
α	-0.87^o	$6.2x10^7$	$5x10^{-6}$
β	1.01^o	$2x10^4$	$3.4x10^{-6}$
Φ	-	800	$1.6x10^{-2}$

Table 2. Error budget mean, accuracy and multiplication factors

The phase uncertainty σ_Φ^2 has been estimated by using equation 1, where N_L and γ are equal to 2x16 (range x azimuth) and 0.7 respectively.
It is worth nothing that the height accuracy is mainly affected by the aircraft roll and by the scene coherence.

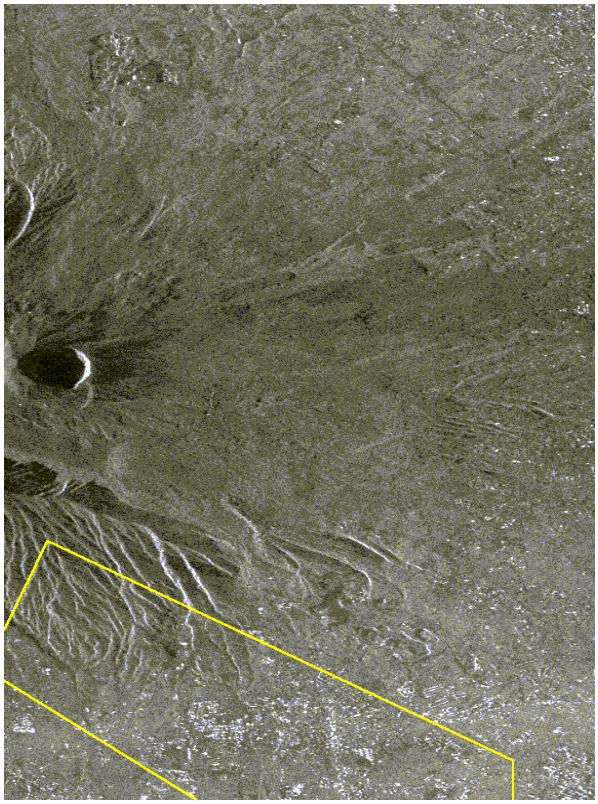

Figure 4. Validation area within the compressed Vesuvius image.

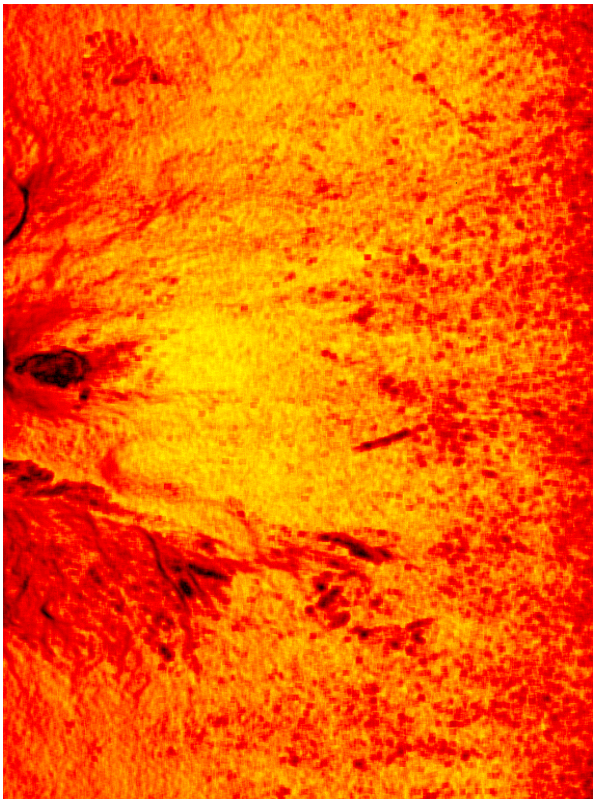

Figure 6. Coherence map: from black (0.2÷0.3) to yellow (0.8÷0.9).

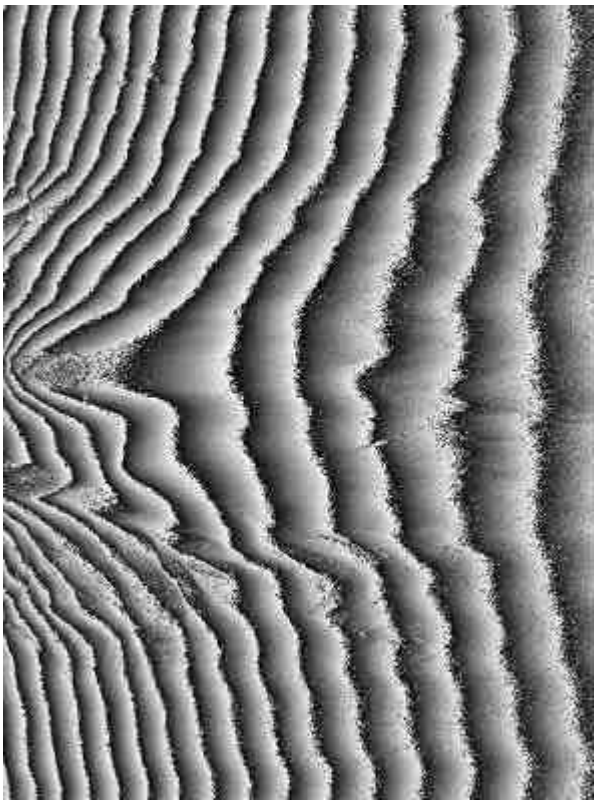

Figure 5. Test-site interferogram.

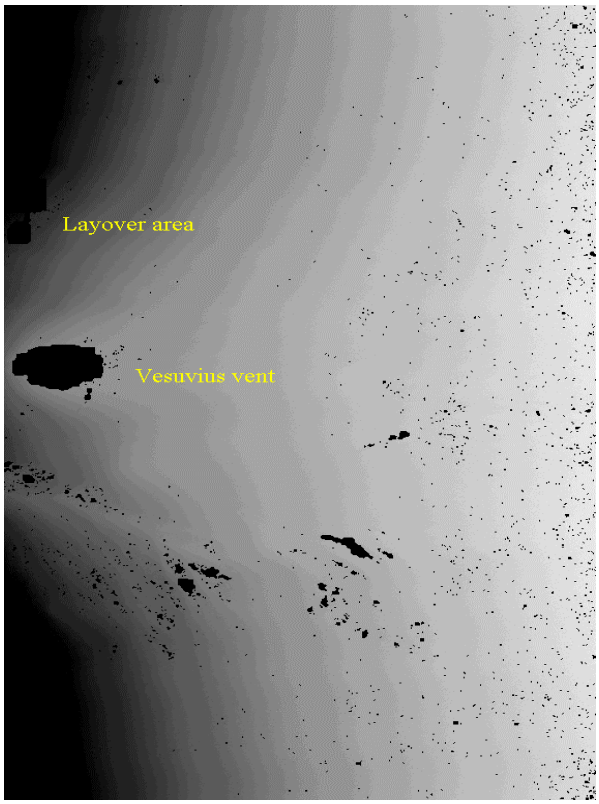

Figure 7. Unwrapped phase image.

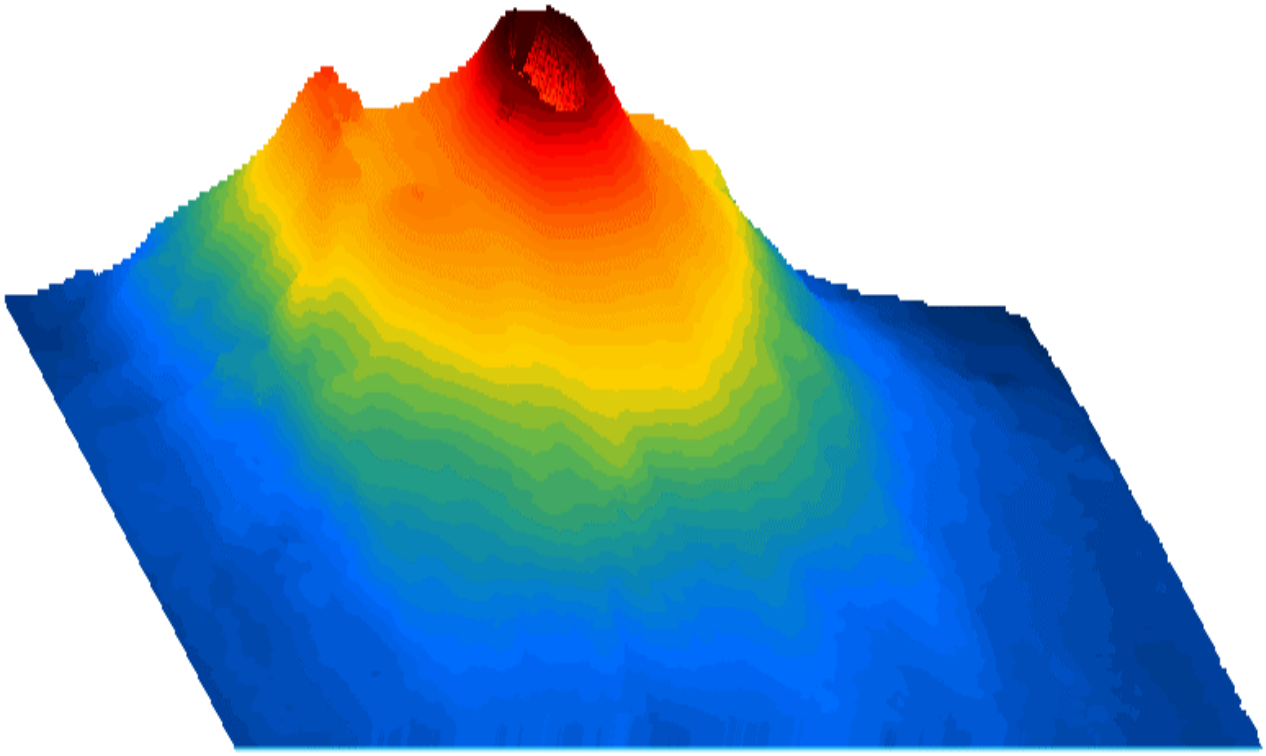

Figure 9. Three dimensional view of the interferometric DEM.

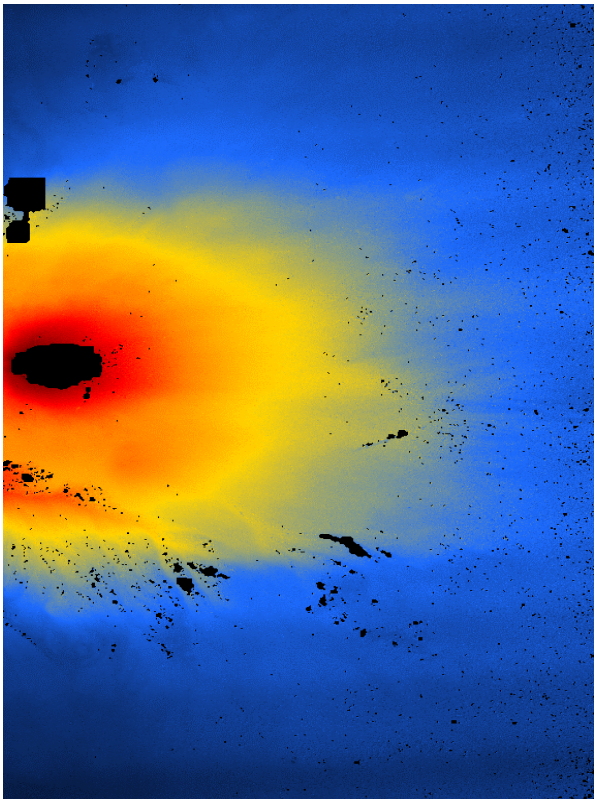

Figure 8. Interferometric DEM: from azure (~50 m) to red (~1200 m).

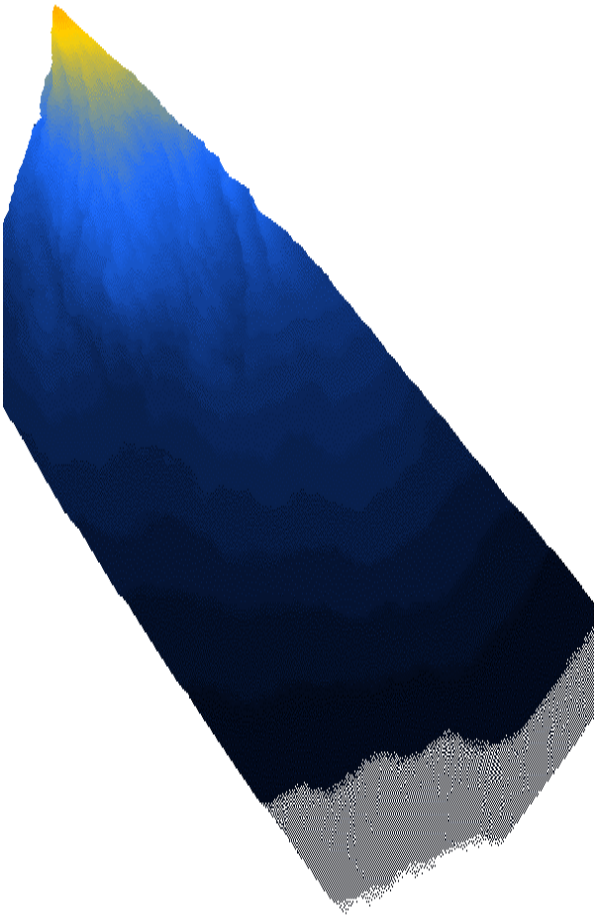

Figure 10. Slant range projection of the photogrammetric DEM: from azure (~50 m) to yellow (~1016 m).

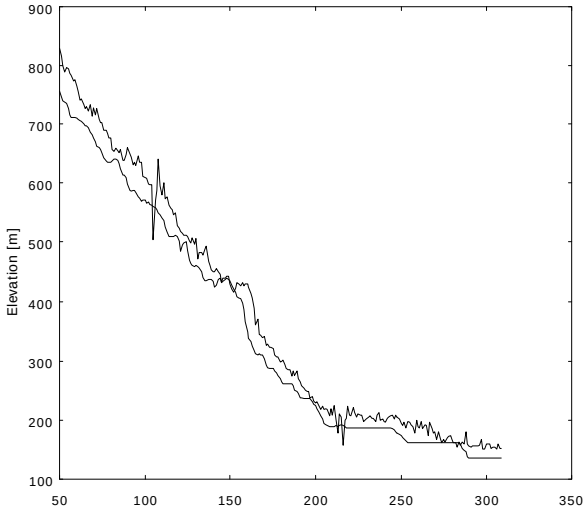

Figure 11. Comparison between two homologous range lines

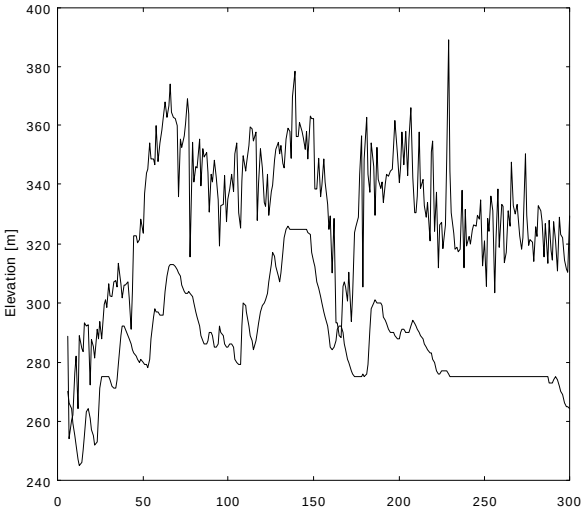

Figure 12. Comparison between two homologous azimuth lines.

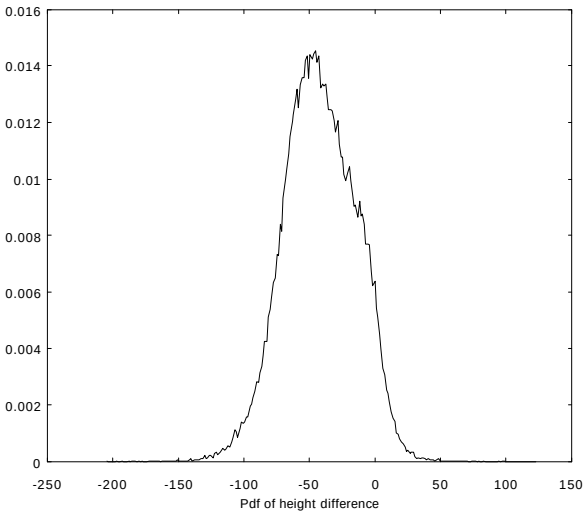

Figure 13. Interferometric DEM height error histogram.

CONCLUSIONS

An end-to-end approach has been presented to process and validate SAR interferometric data. The interferometric DEM and the corresponding photogrammetric DEM at a scale 1:25000 have been compared and a final error of 26 m has been computed, which has been interpreted in terms of the theoretical error budget.

The analysis shows the need of improving several steps of the proposed procedure, by introducing the platform motion compensation both during the image compression and the interferometric height reconstruction.

As far as the validation procedure is concerned, the presented method is extremely powerful and flexible as proved by the results. Nevertheless it is high dependent on the ancillary data accuracy and, therefore, a significant improvement of the height accuracy is expected by using the GPS ancillary data.

ACKNOWLEDGEMENTS

This paper has been carried out under the sponsorship of Italian Space Agency (ASI).

REFERENCES

1. Gabriel, A. K, and Goldstein, R. M., 1988, Crossed orbit interferometry: theory and experimental results from SIR-B. *International Journal of Remote Sensing*, Vol. 9, No. 8, pp.857-872.
2. Graham, L. C., 1974, Synthetic Interferometer Radar For Topographic Mapping. *Proceedings of the IEEE*, Vol. 62, No. 6, pp. 763-768.
3. Zebker, H. A., Madsen, S. N., Martin, J., Wheeler, K. B., Miller, T., and Lou, Y., Alberti, G., Vetrella, S. and Cucci, A., 1992, The TOPSAR Interferometric Radar Topographic Mapping Instrument. *IEEE Transactions on Geoscience and Remote Sensing*, Vol. 30, No. 5, pp. 933-940.
4. Prati, C., Rocca, F., Monti Guarnieri, A., and Damonti, E., 1990, Seismic Migration for SAR Focusing: Interferometrical Applications. *IEEE Transactions on Geoscience and Remote Sensing*, Vol. 28, No. 4, pp. 627-640.
5. Zebker, H. A., and Goldstein, R. M., 1986, Topographic Mapping From Interferometric Synthetic Aperture Radar Observations. *Journal of Geophysical Research*, Vol. 91, No. B5, pp. 4993-4999.
6. Alberti G., Vetrella S., Moccia A., Ponte S. 1993, Analysis and results of the TOPSAR experiment in Southern Italy, *EARSeL Advances in Remote Sensing*, Vol 3 n.1, Sept 1994, pp 2-18
7. Madsen, S. N., Zebker, H. A. and Martin, J., 1993, Topographic mapping using radar interferometry: processing techniques, *IEEE Transactions on Geoscience and Remote Sensing*, Vol. 31, No. 1, pp. 246-256.
8. Goldestein R.M., Zebker H. A. and Werner C. L. 1988, Satellite radar interferometry: two dimensional phase unwrapping, *Radio Science*, 23, pp 713-720

9. Lin Q., Vesecky J.F. and Zebker H.A., 1992. "New Approaches in Interferometric SAR Data Processing", IEEE Trans. on Geoscience and Remote Sensing, vol. 30, no. 3, pp. 560-567.
10. Bone, 1991: "Fourier Fringe analysis: the two-dimensional phase unwrapping problem", Applied Optics, Vol. 30, No. 25, pp. 3627-3632.
11. Rodriguez, E., Maximum likelihood estimation of interferometric phase from distributed targets, *IEEE Transaction on Geoscience and Remote Sensing* (to be published)
12. Vetrella S. and Moccia A, 1988. "A Procedure for Modeling the Terrain Relief by Using Digitised Topographic Maps", Geocarto International, Vol. 3, no. 3, pp. 3-11.